Laser-induced breakdown spectroscopy of ammonia gas with resonant vibrational excitation

Guang Yang, Liu Lei, Tao Wang, Lei Liu, Lisha Fan, Xi Huang, Di Tian, Lan Jiang, Jean-François Silvain, Yongfeng Lu

Optics EXPRESS

Laser-induced breakdown spectroscopy of ammonia gas with resonant vibrational excitation

GUANG YANG,[2,6] LEI LIU,[1,6] TAO WANG,[3] LISHA FAN,[1] XI HUANG,[1] DI TIAN,[2] LAN JIANG,[1,4] JEAN-FRANÇOIS SILVAIN,[1,5] AND YONGFENG LU[1,*]

[1]*Department of Electrical and Computer Engineering, University of Nebraska-Lincoln, Lincoln, NE 68588-0511, USA*
[2]*College of Instrumentation & Electrical Engineering, Jilin University, Changchun, China*
[3]*Department of Mechanical and Electrical Engineering, Civil Aviation University of China, Tianjin, China*
[4]*School of Mechanical Engineering, Beijing Institute of Technology, Beijing, China*
[5]*Institut de Chimie de la Matière Condensée de Bordeaux–ICMCB-CNRS 87, Avenue du Docteur Albert Schweitzer F-33608 Pessac Cedex, France*
[6]*These authors contributed equally to this work*
[*]*ylu2@unl.edu*

Abstract: In this work, laser-induced breakdown spectroscopy (LIBS) of gaseous ammonia (NH_3) molecules on- and off-resonant vibrational excitation was studied in open air. A wavelength-tunable, continuous wave (CW), carbon dioxide (CO_2) laser tuned at a resonant absorption peak (9.219 μm) within the infrared radiation (IR) range was used to resonantly excite the vibration of the N-H wagging mode of ammonia molecules. A pulsed Nd:YAG laser (1064 nm, 15 ns) was used to break down the ammonia gas for plasma imaging and spectral measurements. In this study, plasmas generated with the ammonia molecules without additional CO_2 laser beam irradiation and with additional CO_2 laser beam irradiation with the wavelengths on- and off-resonant vibrational excitation of ammonia molecules were investigated and referred as LIBS, LIBS-RE-ON and LIBS-RE-OFF, respectively. The experimental results showed that the temporal and spatial evolution as well as electron temperature and density of plasmas induced with LIBS and LIBS-RE-OFF were consistent but differed from LIBS-RE-ON. Compared with LIBS and LIBS-RE-OFF, plasmas in LIBS-RE-ON showed larger spatial expansion and enhanced emission after a delay time of 1 μs in this study, as well as significantly enhanced electron temperature by ~ 64%. Time-resolved electron temperatures and densities showed that the emission signal enhancement in LIBS-RE-ON can be primarily attributed to the electron temperature enhancement. Signal enhancement in LIBS indicated improved detection sensitivity. This study could inspire future works on LIBS for gas detection with improved sensitivity and selectivity probably by using ultrafast/intense laser-induced molecular breakdown/ionization with resonant vibrational excitation of molecules.

1. Introduction

Laser-induced breakdown spectroscopy (LIBS), as an optical emission spectroscopy, has been widely applied to determining the elemental composition of solids, liquids, and gases. In LIBS, a pulsed laser beam is focused to locally break down the target material and induce plasmas which emit chemical elemental characteristic photons during the cooling process. The plasma optical emission is collected and coupled into a spectrometer for spectroscopic analysis to provide qualitative or quantitative information about the material's elemental composition [1–3]. Characteristics of the LIBS technology include no sample preparation, nearly nondestructive

analysis, simultaneous multielement analysis, remote detection, and rapid in situ analysis. Hence, LIBS has widespread applications in geology, biomedicine, pharmaceuticals, environmental contamination, plasma chemistry, industrial monitoring, etc. [3]. In addition to the analyses used most often for solids and liquids, LIBS has also been used for gas analyses in applications of laser ignition [4], combustion diagnostics [5–9], and laser plasma chemistry [10,11]. However, to the authors' knowledge, LIBS for gas analyses has been reported only for molecules in natural states without resonant vibrational excitation. No studies about LIBS for molecules under resonant vibrational excitation have been reported. Therefore, this study will fill the current gap by investigating LIBS of gaseous molecules under resonant vibrational excitation. In addition, how the resonant vibrational excitation will affect the molecular breakdown/ionization process in various laser fields is interesting to be explored. Hence, this study will partially fill the gap of LIBS for gas detection under resonant vibrational excitation and provide inspirations for future research to explore how the resonant vibrational excitation will affect the molecular breakdown/ionization process as well as spectroscopy in various laser fields. Altered molecular ionization process from resonant vibrational excitation might result in composition variation of molecular fragments and play important roles in laser-assisted chemical reactions, such as laser-assisted growth of high-quality diamond [12] and laser-assisted low-temperature growth of gallium nitride [13].

In this study, laser-induced breakdown of gaseous ammonia (NH_3) molecules with no carbon dioxide (CO_2) laser beam irradiation and with CO_2 laser beam irradiation with wavelengths on- and off-resonant (LIBS-RE-OFF) vibrational excitation of ammonia molecules were investigated and referred as LIBS, LIBS-RE-ON, and LIBS-RE-OFF, respectively. A wavelength-tunable, continuous wave (CW) CO_2 laser tuned to specific wavelengths of 9.219 and 10.591 μm, respectively, was used for on- and off-resonant vibrational excitation of ammonia molecules. A pulsed Nd:YAG laser (1064 nm, 15 ns) was used to break down the ammonia gas and induce plasmas. The plasma optical emission was collected and coupled into a spectrometer and a camera for spectroscopy and imaging measurements, respectively. Time-resolved spectra of the laser-induced plasmas were studied to explore the LIBS signal change with the gaseous molecule on- and off-resonant vibrational excitation. Fast imaging was used to investigate the spatial evolution of plasmas. Temporal evolution of the electron temperature and density of laser-induced plasmas were also studied to reveal the plasma property changes in LIBS, LIBS-RE-ON, and LIBS-RE-OFF, respectively.

2. Experiment setup

A schematic diagram of the experiment setup for LIBS of gaseous ammonia molecules in open air as well as with on- and off-resonant vibrational excitation of ammonia molecules is shown in Fig. 1. The gaseous ammonia was ejected vertically from a nozzle into the air with a flow rate of 80 standard cubic centimeters per minute (sccm). A flexible exhaust pipe was fixed 10 cm below the nozzle to draw away the excessive ammonia gas. A commercial Nd:YAG laser (Quantel DRL, 15 ns, 1064 nm) operated with a pulse energy of 630 mJ and a repetition rate of 5 Hz was horizontally focused by a plano-convex lens (diameter = 50.8 mm, focal length = 75 mm) to a spot size of 0.3 mm in diameter at a location 1.5 mm below the nozzle to induce breakdown of the gaseous ammonia. A wavelength-tunable CW CO_2 laser (PRC Inc., 9.2 ~ 10.9 μm) beam was horizontally focused to a spot size of 1 mm in diameter by a zinc selenide (ZnSe) convex lens (focal length = 200 mm) and orthogonal to the Nd:YAG laser beam in the focal plane. The plasma emissions were collected by a light collector (Andor Technology, ME-OPT-0007) which was fixed in the horizontal plane with an angle of 45 degrees clockwise along the CO_2 laser beam direction. The plasma emission collected was coupled into a spectrometer through an optical fiber with a 200 μm core diameter. The spectrometer consists of a spectrograph (Andor Tech., Shamrock 303i) and an intensified charge-coupled device (ICCD) detector (Andor Tech.,

DH-712) attached to the exit focal plane of the spectrograph. The ICCD detector was externally triggered by the Nd:YAG laser for temporal synchronization. The gate delay and gate width of the ICCD detector are adjustable for temporal measurements. Three gratings of 150, 1200, and 2400 l/mm are included in the spectrometer. The 150 l/mm grating was used for all spectroscopy measurements in this study. An ICCD camera, comprised of a Nikon micro lens (105 mm, f/2.8 D) and an attached ICCD detector (Andor Tech., DH-734), was fixed in the horizontal plane with an angle of 135 degrees clockwise along the CO_2 laser beam direction and used for fast imaging.

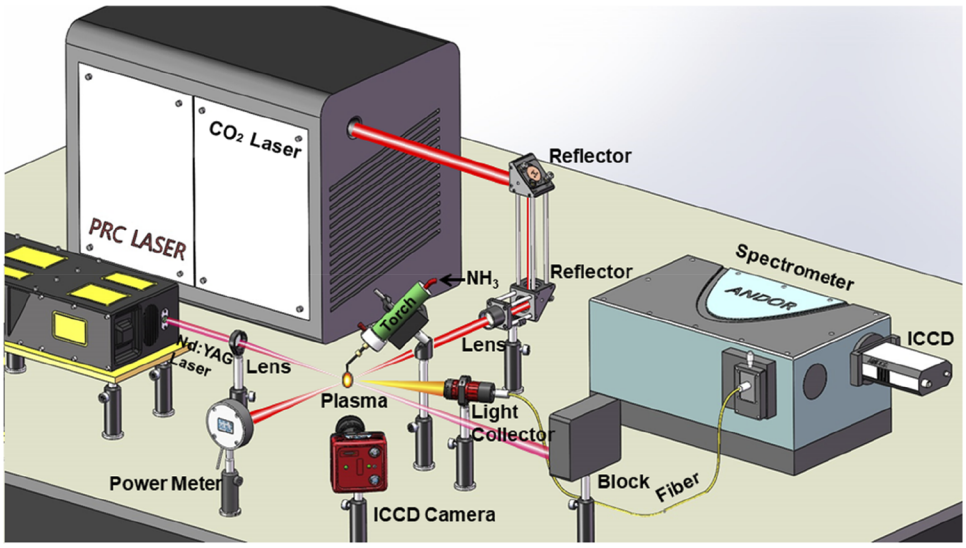

Fig. 1. Schematic diagram of the experiment setup for laser-induced breakdown spectroscopy of ammonia molecules as well as with on- and off-resonant vibrational excitation of ammonia molecules.

In this study, LIBS, LIBS-RE-ON, and LIBS-RE-OFF refer to ammonia gas without additional CO_2 laser beam irradiation, with the CO_2 laser beam irradiation at a wavelength of 9.219 μm (on-resonant vibrational excitation of the N-H wagging mode of ammonia molecules), and with the CO_2 laser beam irradiation at a wavelength of 10.591 μm (default CO_2 laser wavelength,

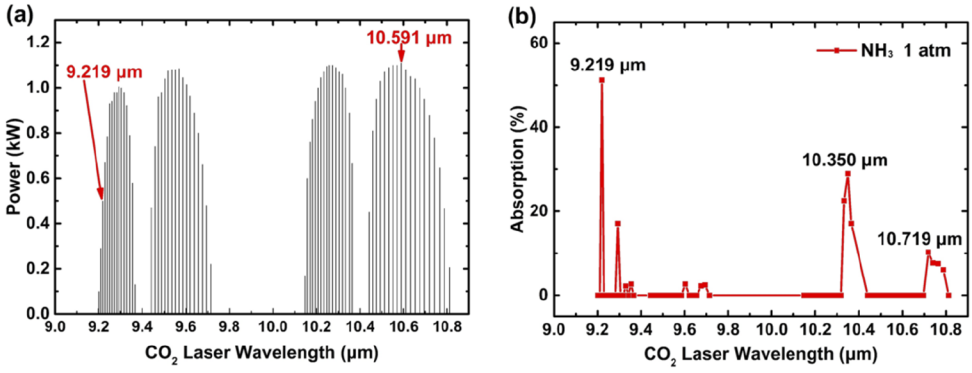

Fig. 2. (a) The relationship between the output wavelength and maximum power of the CO_2 laser; (b) the absorption spectrum of the gaseous ammonia in open air at atmospheric pressure within the CO_2 laser wavelength tunable range of 9.2–10.8 μm.

off-resonant vibrational excitation of ammonia molecules), respectively. For both on- and off-resonant vibrational excitation, the output power of the CO_2 laser used was 33 watts (W). The relationship between the output wavelength and maximum power of the CO_2 laser is shown in Fig. 2(a). The absorption spectrum of the gaseous ammonia within the CO_2 laser wavelength tunable range was measured in open air at atmospheric pressure and is shown in Fig. 2(b).

3. Results and discussion

3.1. Spectra and images of ammonia plasmas

Optical emission spectra and images of the laser-induced gaseous ammonia plasma at different delay times were measured by the spectrometer and ICCD camera, respectively, to investigate the spectral and spatial evolution of the plasmas. Figure 3 shows the plasma emission spectra measured at a delay time of 2 μs in LIBS (black line), LIBS-RE-ON (red line), and LIBS-RE-OFF (blue line). The spectral intensities in LIBS and LIBS-RE-OFF were consistent but differed from LIBS-RE-ON spectral intensities. Enhanced atomic emission signals from both hydrogen and nitrogen were observed in LIBS-RE-ON.

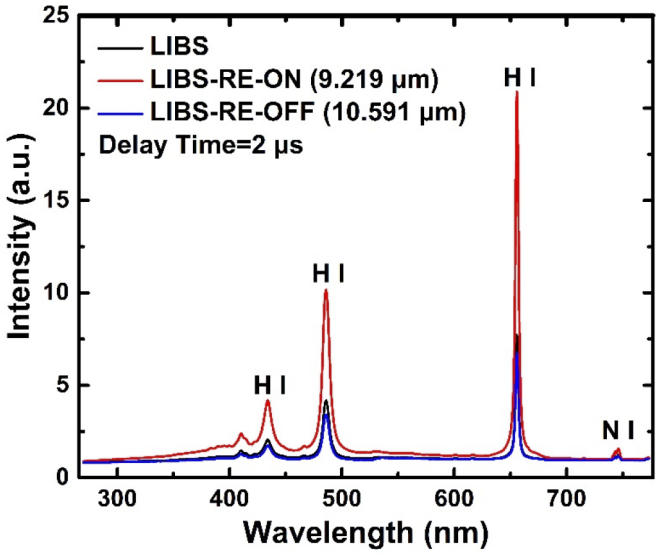

Fig. 3. Spectra of plasma optical emission in LIBS (black line), LIBS-RE-ON (red line), and LIBS-RE-OFF (blue line) measured at the delay time of 2 μs.

To investigate the plasma spectral evolution, optical emission spectra of plasmas during the observation time window of 1 ~ 15 μs were measured using a gate width of 1 μs and a gate step of 1 μs. Peak intensities of the atomic emission line of H I 656.3 nm and N I 746.8 nm at different delay times in LIBS (black squares), LIBS-RE-ON (red dots), and LIBS-RE-OFF (blue triangles) are shown in Figs. 4(a) and 4(b), respectively. As shown in Fig. 4, the evolution of peak intensities of both H I 656.3 nm and N I 746.8 nm in LIBS and LIBS-RE-OFF were consistent but differed from LIBS-RE-ON. In LIBS-RE-ON, enhanced signals of H I 656.3 nm and N I 746.8 nm were both observed within the delay time range of 1 ~ 6 μs. In addition, the signal enhancement factor in LIBS-RE-ON is delay time dependent. For example, the signal of H I 656.3 nm is enhanced by 2 - 3 times during the delay time rang of 1 ~ 4 μs, which decreases to 1 - 2 times during the delay time range of 5 ~ 6 μs. No signal enhancement is observed after 6 μs in this study. Causes for the signal enhancement will be explained later in the content by studying the evolution of the plasma properties.

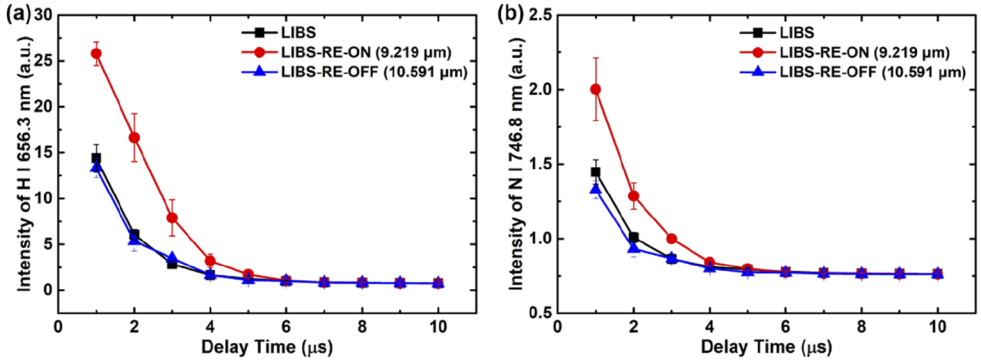

Fig. 4. Peak intensities of the atomic emission lines of (a) H I 656.3 nm and (b) N I 746. 8 nm at different delay times in LIBS (black squares), LIBS-RE-ON (red dots), and LIBS-RE-OFF (blue triangles).

Plasma images during the observation time window of 1 ~ 15 μs were measured using a gate width of 0.06 μs and a gate step of 1 μs to investigate the spatial evolution of the laser-induced plasmas. Figures 5(a)–5(c) show the images of plasmas generated in LIBS, LIBS-RE-OFF, and LIBS-RE-ON, respectively, at the selected delay times of 1, 3, 5, and 7 μs, respectively. At each delay time, the maximum intensity of the plasma images in LIBS, LIBS-RE-OFF, and LIBS-RE-ON were calibrated to the same scale for comparison. Spatial evolution of plasmas both in LIBS and LIBS-RE-OFF were similar but differed from LIBS-RE-ON, similar to the phenomenon in the previous spectral analyses. Compared with LIBS and LIBS-RE-OFF, the plasmas in LIBS-RE-ON showed larger spatial sizes as well as enhanced emission intensities during the observation time window, such as shown at the delay times between 3 and 5 μs.

3.2. Electron temperature and density of plasmas

The electron temperature and density of plasmas during the observation time window of 1 ~ 10 μs were calculated to reveal the spectral characteristics. Figures 6(a) and 6(b) show the evolution of electron temperature and density, respectively, in LIBS (black squares), LIBS-RE-ON (red dots), and LIBS-RE-OFF (blue triangles). With the assumption of local thermodynamic equilibrium, the plasma temperature can be calculated from the relative intensity ratio of spectral lines from the same element ionization stage according to the Boltzmann distribution, using the equation of [3,14,15],

$$\frac{I_1}{I_2} = \left(\frac{g_1 A_1}{g_2 A_2}\right)\left(\frac{\lambda_2}{\lambda_1}\right) exp\left[\frac{-(E_1 - E_2)}{\kappa T_e}\right] \quad (1)$$

where I_i and λ_i are the integrated line intensity and wavelength, respectively. Symbols of A_i, g_i, and E_i are the transition probability, statistical weight, and excited energy for the upper level, respectively. Symbols of κ and T_e are the Boltzmann constant and the electron temperature of the plasma, respectively. A pair of spectral lines of H I 656.3 nm (combined from H I 656.271, 656.272, and 626.285 nm) and H I 486.1 nm (combined from H I 486.128, 486.129, and 486.136 nm) were used for electron temperature calculation. During electron temperature calculation, the multiplications of A_i and g_i of each atomic line were summed, respectively, for the two chosen lines [15]. The parameters of atomic lines used for temperature calculation are shown in Table 1 [16].

The emission line of H I 656.3 nm was used to obtain the electron density, N_e, using the following expression given by Ashkenazy [17,18],

$$N_e = 8.02 \times 10^{12} (\Delta\lambda_{1/2}/\alpha_{1/2})^{3/2} \text{ cm}^{-3} \quad (2)$$

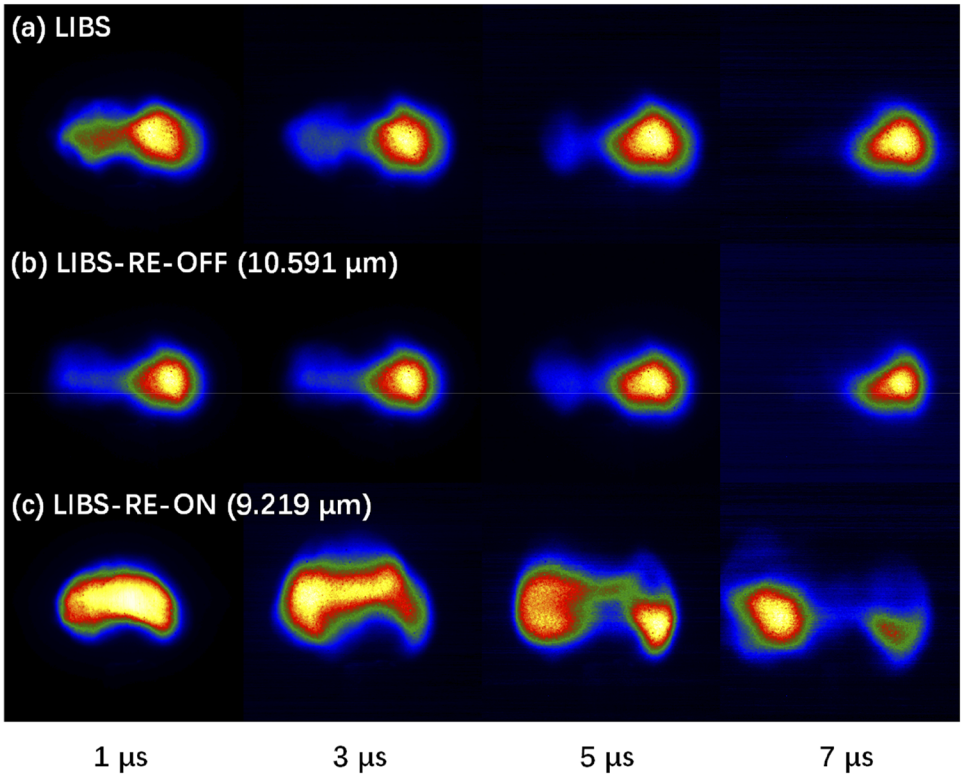

Fig. 5. Images of plasmas generated in (a) LIBS, (b) LIBS-RE-OFF, and (c) LIBS-RE-ON, respectively, at the delay times of 1, 3, 5, and 7 μs.

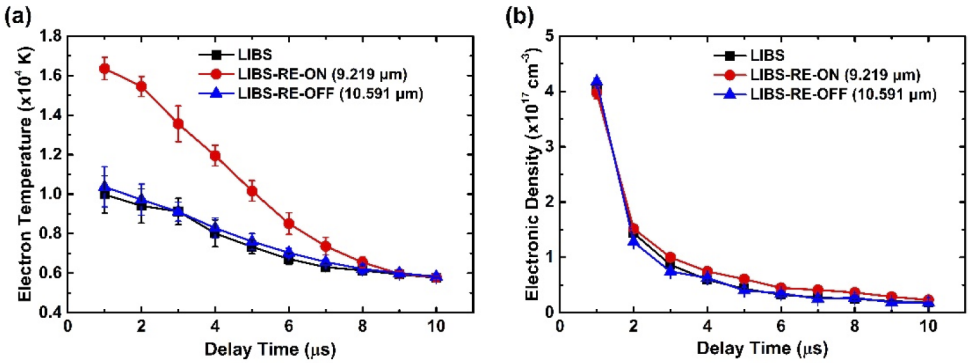

Fig. 6. Temporal evolution of (a) electron temperature and (b) electron density of plasmas generated in LIBS (black squares), LIBS-RE-ON (red dots), and LIBS-RE-OFF (blue triangles).

where $\Delta\lambda_{1/2}$ is the full width at half maximum (FWHM) of the H I 656.3 nm line, and $\alpha_{1/2}$ is half the width of the reduced Stark profiles in units of Å. The values of $\alpha_{1/2}$ for the Balmer series can be found in several citations [19,20]. For more information about the electron temperature and density calculation of plasmas generated from laser-induced breakdown of gases, please refer to Refs. [21–23].

Table 1. Parameters of atomic lines used for plasma temperature calculation.

Wavelength (nm)	Excited upper level energy E_i (cm^{-1})	Transition probability A_i (s^{-1})	Statistical weight for upper level g_i
486.128	102824	0.1719 e + 08	4
486.129	102824	0.0967 e + 08	4
486.136	102824	0.2063 e + 08	6
656.271	97492	0.5388 e + 08	4
656.272	97492	0.2245 e + 08	2
656.285	97492	0.6465 e + 08	6

As shown in Fig. 6, the temporal evolution of the electron temperature of plasmas generated in LIBS and LIBS-RE-OFF were consistent but differed from LIBS-RE-ON. Compared with LIBS and LIBS-RE-OFF, plasmas generated in LIBS-RE-ON possessed higher electron temperatures, such as those enhanced from $\sim 1.0\times10^4$ K in LIBS to $\sim 1.6\times10^4$ K in LIBS-RE-ON at the delay time of 1 μs, with a temperature enhancement of ~ 64%. However, the temporal evolution of the electron density of plasmas generated in LIBS, LIBS-RE-OFF, and LIBS-RE-ON were close to each other except for a tiny increase in LIBS-RE-ON after a delay time of 3 μs. Therefore, the spectral signal enhancement in LIBS-RE-ON can primarily be attributed to the increase in the electron temperature of plasmas.

The electron temperature evolution in LIBS-RE-ON was similar to some previous studies about laser-induced plasma evolution in a high-temperature flame atmospheric environment, which showed that enhanced electron temperatures were observed in the high temperature atmospheric environment [24,25]. The enhanced electron temperature in LIBS-RE-ON is presumably due to the temperature increase in gaseous ammonia through absorption of the CO_2 laser energy at the resonant vibrational excitation wavelength of ammonia. Therefore, a real-time datalogging thermometer (Oakton, Temp-360, temperature range −210 to 1210 °C) was used to measure the ammonia gas temperature under the conditions of without CO_2 laser irradiation, with CO_2 laser irradiation at a power of 33 W at the wavelength of 10.591 μm (off-resonant) and 9.219 μm (on-resonant), respectively. As shown in Fig. 7, the sensor of the thermometer was fixed 5 mm below the nozzle to measure the ammonia gas temperature before breakdown. Under this condition, the measured temperature of the ammonia gas without CO_2 laser irradiation was 20 ± 0.5 °C. With CO_2 laser irradiation at a power of 33 W at the wavelengths of 10.591 μm (off-resonant) and 9.219 μm (on-resonant), the measured temperature of the ammonia gas was 27 ± 0.9 °C and 180 ± 13 °C, respectively. With resonant vibrational excitation of the ammonia molecules, the ammonia gas temperature increased by around 160 °C before breakdown in this study. Hence, the enhancement of the electron temperature of the laser-induced plasma in LIBS-RE-ON was probably primarily due to the ammonia gas temperature increase before breakdown. In more detail, the gas temperature increase before breakdown in LIBS-RE-ON provides a higher temperature atmospheric environment in which the root mean square (RMS) velocity of electrons will be increased, which could result in enhanced avalanche breakdown process and hence enhanced electron temperature. Compared with the avalanche ionization mechanism in ns laser-induced breakdown process [26], the molecular breakdown/ionization mechanism differs primarily as multiphoton/tunneling ionization in ultrafast/intense laser fields [27–29]. Hence, under resonant vibrational excitation of gaseous molecules, different effects on the molecular breakdown/ionization in the aspects of plasma properties, composition of molecular fragments, and spectroscopy in an ultrafast/intense laser field could be expected, which will be interesting for future studies.

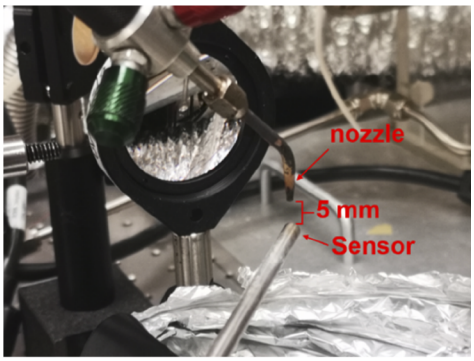

Fig. 7. The sensor of a thermometer fixed 5 mm below the nozzle for measurements of the ammonia gas temperature.

4. Summary

In this study, laser-induced breakdown of NH_3 under LIBS (no CO_2 laser beam irradiation), LIBS-RE-ON (with CO_2 laser beam irradiation at 9.219 μm, on-resonant vibrational excitation of ammonia), and LIBS-RE-OFF (with CO_2 laser beam irradiation at 10.591 μm, off-resonant vibrational excitation of ammonia) was studied in open air. The spectral and spatial evolution of plasmas generated in LIBS, LIBS-RE-ON, and LIBS-RE-OFF were investigated by spectral analyses and plasma imaging. The spectral and spatial evolution of plasmas generated in LIBS and LIBS-RE-OFF were consistent but differed from LIBS-RE-ON. Compared with LIBS and LIBS-RE-OFF, plasmas generated in LIBS-RE-ON showed enhanced atomic emission signals and larger spatial plasma size. The electron temperature and density of plasmas were calculated to help explain the atomic emission signal enhancement in LIBS-RE-ON. The same as the tendency in the spectral evolution, plasma properties of electron temperature and electron density in LIBS and LIBS-RE-OFF were consistent but differed from LIBS-RE-ON. Compared with LIBS and LIBS-RE-OFF, plasmas generated in LIBS-RE-ON showed enhanced electron temperature but almost the same electron density during the observation time window of 1 ~ 10 μs, such as the electron temperature enhanced from ~ 1.0×10^4 K in LIBS to ~ 1.6×10^4 K (enhanced by ~ 64%) in LIBS-RE-ON at the delay time of 1 μs. Therefore, the enhanced atomic emission signals of spectra in LIBS-RE-ON can be primarily attributed to the enhancement of electron temperatures. The electron temperature enhancement of the plasma in LIBS-RE-ON is probably due to the temperature increase in the gaseous ammonia through absorption of the CW CO_2 laser power at the on-resonant vibrational excitation wavelength of ammonia before laser breakdown of the gas. Enhanced emission signals in LIBS generally indicate improved sensitivity. This study could inspire future works on LIBS for gas detection with improved sensitivity probably by using ultrafast/intense laser-induced LIBS with resonant vibrational excitation of molecules.

Acknowledgments

The authors gratefully acknowledge Zhipeng Wu in the Laser-Assisted Nano Engineering (LANE) lab at the University of Nebraska-Lincoln (UNL) for technical assistance in CO_2 laser operation training.

Disclosures

The authors declare no conflicts of interest.

References

1. R. Noll and SpringerLink (Online service), *Laser-Induced Breakdown Spectroscopy: Fundamentals and Applications* (2012), pp. 1 online resource (XII, 544 p.).
2. J. P. Singh and S. N. Thakur, *Laser-induced breakdown spectroscopy*, 1st ed. (Elsevier, 2007), pp. xxiv, 429 p.
3. A. W. Miziolek, V. Palleschi, and I. Schechter, *Laser-induced breakdown spectroscopy (LIBS) : fundamentals and applications* (Cambridge University Press, 2006), pp. xvii, 620 p.
4. Y. L. Chen and J. W. L. Lewis, "Visualization of laser-induced breakdown and ignition," Opt. Express **9**(7), 360–372 (2001).
5. P. Stavropoulos, A. Michalakou, G. Skevis, and S. Couris, "Laser-induced breakdown spectroscopy as an analytical tool for equivalence ratio measurement in methane-air premixed flames," Spectrochim. Acta, Part B **60**(7-8), 1092–1097 (2005).
6. J. Kiefer, J. W. Troger, Z. S. Li, T. Seeger, M. Alden, and A. Leipertz, "Laser-induced breakdown flame thermometry," Combust. Flame **159**(12), 3576–3582 (2012).
7. J. Kiefer, B. Zhou, Z. S. Li, and M. Alden, "Impact of plasma dynamics on equivalence ratio measurements by laser-induced breakdown spectroscopy," Appl. Opt. **54**(13), 4221–4226 (2015).
8. P. S. Hsu, M. Gragston, Y. Wu, Z. L. Zhang, A. K. Patnaik, J. Kiefer, S. Roy, and J. R. Gord, "Sensitivity, stability, and precision of quantitative Ns-LIBS-based fuel-air-ratio measurements for methane-air flames at 1-11 bar," Appl. Opt. **55**(28), 8042–8048 (2016).
9. Y. Wu, M. Gragston, Z. L. Zhang, P. S. Hsu, N. B. Jiang, A. K. Patnaik, S. Roy, and J. R. Gord, "High-pressure 1D fuel/air-ratio measurements with LIBS," Combust. Flame **198**, 120–129 (2018).
10. D. Babankova, S. Civis, and L. Juha, "Chemical consequences of laser-induced dielectric breakdown in molecular gases," Chem Listy **99**, 109–115 (2005).
11. D. Babankova, S. Civis, and L. Juha, "Chemical consequences of laser-induced breakdown in molecular gases," Prog. Quantum Electron. **30**(2-3), 75–88 (2006).
12. L. S. Fan, Y. S. Zhou, M. X. Wang, Y. Gao, L. Liu, J. F. Silvain, and Y. F. Lu, "Resonant vibrational excitation of ethylene molecules in laser-assisted diamond deposition," Laser Phys. Lett. **11**(7), 076002 (2014).
13. H. R. Golgir, Y. S. Zhou, D. W. Li, K. Keramatnejad, W. Xiong, M. M. Wang, L. J. Jiang, X. Huang, L. Jiang, J. F. Silvain, and Y. F. Lu, "Resonant and nonresonant vibrational excitation of ammonia molecules in the growth of gallium nitride using laser-assisted metal organic chemical vapour deposition," J. Appl. Phys. **120**(10), 105303 (2016).
14. J. Sneddon, T. L. Thiem, and Y.-I. Lee, *Lasers in analytical atomic spectroscopy* (John Wiley & Sons, 1996).
15. X. N. He, W. Hu, C. M. Li, L. B. Guo, and Y. F. Lu, "Generation of high-temperature and low-density plasmas for improved spectral resolutions in laser-induced breakdown spectroscopy," Opt. Express **19**(11), 10997–11006 (2011).
16. H. D. Vora and N. B. Dahotre, "Surface topography in three-dimensional laser machining of structural alumina," J. Manuf. Process. **19**, 49–58 (2015).
17. J. Ashkenazy, R. Kipper, and M. Caner, "Spectroscopic Measurements of Electron-Density of Capillary Plasma Based on Stark-Broadening of Hydrogen Lines," Phys. Rev. A **43**(10), 5568–5574 (1991).
18. C. Colon, M. I. de Andres-Garcia, C. Moreno-Diaz, A. Alonso-Medina, J. A. Porro, I. Angulo, and J. L. Ocana, "Experimental Determination of Electronic Density and Temperature in Water-Confined Plasmas Generated by Laser Shock Processing," Metals (Basel, Switz.) **9**(7), 808 (2019).
19. H. Griem, *Spectral line broadening by plasmas* (Elsevier, 2012).
20. P. Kepple and H. R. Griem, "Improved Stark profile calculations for the hydrogen lines H α, H β, H γ, and H δ," Phys. Rev. **173**(1), 317–325 (1968).
21. D. Surmick and C. Parigger, "Empirical formulae for electron density diagnostics from Hα and Hβ line profiles," Int. Rev. At. Mol. Phys. **5**, 73–81 (2014).
22. A. K. Patnaik, Y. Wu, P. S. Hsu, M. Gragston, Z. L. Zhang, J. R. Gord, and S. Roy, "Simultaneous LIBS signal and plasma density measurement for quantitative insight into signal instability at elevated pressure," Opt. Express **26**(20), 25750–25760 (2018).
23. A. Rao, M. Gragston, A. K. Patnaik, P. S. Hsu, and M. B. Shattan, "Measurement of electron density and temperature from laser-induced nitrogen plasma at elevated pressure (1-6 bar)," Opt. Express **27**(23), 33779–33788 (2019).
24. L. Liu, S. Li, X. N. He, X. Huang, C. F. Zhang, L. S. Fan, M. X. Wang, Y. S. Zhou, K. Chen, L. Jiang, J. F. Silvain, and Y. F. Lu, "Flame-enhanced laser-induced breakdown spectroscopy," Opt. Express **22**(7), 7686–7693 (2014).
25. L. Liu, X. Huang, S. Li, Y. Lu, K. Chen, L. Jiang, J. F. Silvain, and Y. F. Lu, "Laser-induced breakdown spectroscopy enhanced by a micro torch," Opt. Express **23**(11), 15047–15056 (2015).
26. S. Musazzi and U. Perini, *Laser-Induced Breakdown Spectroscopy : Theory and Applications*, Springer Series in Optical Sciences, (Springer, 2014), pp. 1 online resource (XXII, 565 p.).
27. P. S. Hsu, A. K. Patnaik, A. J. Stolt, J. Estevadeordal, S. Roy, and J. R. Gord, "Femtosecond-laser-induced plasma spectroscopy for high-pressure gas sensing: Enhanced stability of spectroscopic signal," Appl. Phys. Lett. **113**(21), 214103 (2018).
28. K. Ostrikov, F. Beg, and A. Ng, "Colloquium: Nanoplasmas generated by intense radiation," Rev. Mod. Phys. **88**(1), 011001 (2016).
29. J. Muth-Bohm, A. Becker, and F. H. M. Faisal, "Suppressed molecular ionization for a class of diatomics in intense femtosecond laser fields," Phys. Rev. Lett. **85**(11), 2280–2283 (2000).